Orbital Overlap and Antiferromagnetic Coupling in Substituted Tetraphenylporphinatomanganate(III) Tetracyanoethenide Based Magnets. The Importance of $\sigma-d_{z^2}-p_z$ Overlap

Erik J. Brandon,[1a] Christian Kollmar,*[,1b] and Joel S. Miller*[,1a]

Contribution from the Department of Chemistry, University of Utah, Salt Lake City, Utah 84112-0850, and the Physik Department, Theoretische Physik T38, Technische Universität München, James Franck Strasse, D-85748 Garching, Germany

Received October 2, 1997

Abstract: A correlation between the orientation of $[TCNE]^{\bullet-}$ (TCNE = tetracyanoethylene) bound to a $[Mn^{III}(por)]^+$ (por = substituted *meso*-tetraphenylporphyrin) and the magnitude of magnetic coupling for a series of previously prepared [Mn(por)][TCNE]·2PhMe linear-chain molecule-based ferrimagnets has been identified. The tetraphenylporphyrin (H_2TPP), tetrakis(4-chlorophenyl)porphyrin (H_2TClPP), tetrakis(4-methoxyphenyl)-porphyrin (H_2TOMePP), tetrakis(2-fluorophenyl)porphyrin (H_2TFPP), and tetrakis(3,5-di-*tert*-butyl-4-hydroxyphenyl)porphyrin (H_2TP′P) ligands have all been utilized. Previous structural determinations as the ditoluene solvates indicate that the Mn−N distance varies ∼2.6%, while the $Mn-(N-C)_{TCNE}$ bond angle varies by as much as 25.2% from the mean values over this series of compounds. Hence the overlap between the $[TCNE]^{\bullet-}$ π^* SOMO and the Mn^{III} SOMO d orbitals plays a significant role in controlling the magnetic properties. From molecular orbital overlap considerations, as determined from semiempirical INDO/SCF calculations, the expected $d_\pi-\pi^*$ ($d_\pi = d_{xz}, d_{yz}$) overlap is not as important as the σ-$d_{z^2}-\pi^*$ overlap between Mn^{III} and the $[TCNE]^{\bullet-}$. Furthermore, the greater the deviation from 90° for the dihedral angle between the mean MnN_4 $[Mn(por)]^+$ plane and the $[TCNE]^{\bullet-}$ mean plane increases the $\sigma-d_{z^2}/p_z$ overlap between Mn^{III} and the $[TCNE]^{\bullet-}$ leading to an increased intrachain coupling as the angle is decreased. An increase in the T_{min} (the temperature at which the minima in the temperature dependence of the moment occurs) is observed as this angle becomes more acute, reflecting the stronger magnetic coupling. This suggests systems with smaller $Mn(por)^+/[TCNE]^{\bullet-}$ dihedral and $Mn-(N-C)_{TCNE}$ bond angles should have enhanced intrachain magnetic coupling, J_{intra}, leading to higher T_c's. Pressure may force such systems to have reduced angles and also lead to higher T_c's.

Introduction

The preparation and characterization of molecule-based magnets are of current interest; however, details of the magnetic coupling mechanisms have been elusive.[2,3] Such materials often combine long-range magnetic order with the inherent physical properties of molecular solids (i.e., solubility in organic solvents, low densities, etc.), and much attention has focused toward controlling the magnetic properties through the flexibility of low-temperature organic synthetic methodologies. This has been achieved with, for example, the amorphous $V(TCNE)_x{\cdot}y$(solvent) magnet (where TCNE = tetracyanoethylene) in which the magnetization and T_c may be controlled by use of different preparative solvents and/or starting materials.[4] When dichloromethane is used, a magnet displaying a spontaneous moment and hysteresis above room temperature is obtained. Since this is the only room-temperature magnet to date in which an organic radical actively participates in the magnetic ordering, we are interested in understanding the specific nature of the metal−radical interaction. However, due to the insolubility of this material, a single-crystal X-ray analysis has not been possible. On the basis of IR data, it is surmised the $[TCNE]^{\bullet-}$ is directly bound to up to four V's.

(1) (a) University of Utah. (b) Technische Universität München.

(2) Proceedings on the Conference on Ferromagnetic and High Spin Molecular Based Materials. Miller, J. S., Dougherty, D. A., Eds.; *Mol. Cryst., Liq. Cryst.* **1989**, *176.* Proceedings on the Conference on Molecular Magnetic Materials. Kahn, O., Gatteschi, D., Miller, J. S., Palacio, F., Eds.: *NATO ARW Molecular Magnetic Materials* **1991**, *E198*. Proceedings on the Conference on the Chemistry and Physics of Molecular Based Magnetic Materials. Iwamura, H., Miller, J. S., Eds.; *Mol. Cryst. Liq. Cryst.* **1993,** *232/233*. Proceedings on the Conference on Molecule-based Magnets; Miller, J. S., Epstein, A. J., Eds.; *Mol. Cryst. Liq. Cryst.* **1995**, *271−274*. Proceedings on the Conference on Molecular-Based Magnets. Itoh, K., Takui, T., Miller, J. S. Guest Editors; *Mol. Cryst. Liq. Cryst.* **1997**, *305−306*. Turnbull, M. M., Sugimoto, T., Thompson, L. K., Eds. *A.C.S. Sym. Ser.* **1996**, *644*.

(3) Reviews: (a) Buchachenko, A. L. *Russ. Chem. Rev.* **1990**, *59*, 307; *Usp. Khim.* **1990**, *59*, 529. Kahn, O. *Struct. Bonding* **1987**, *68*, 89. Kahn, O. *Molecular Magnetism*; VCH Publishers: New York, 1993. (b) Caneschi, A.; Gatteschi, D.; Sessoli, R.; Rey, P. *Acc. Chem. Res.* **1989**, *22*, 392. Gatteschi, D. *Adv. Mater.* **1994**, *6*, 635. (c) Miller, J. S.; Epstein, A. J.; Reiff, W. M. *Acc. Chem. Res.* **1988**, *21*, 114. Miller, J. S.; Epstein, A. J.; Reiff, W. M. *Science* **1988**, *240*, 40. Miller, J. S.; Epstein, A. J.; Reiff, W. M. *Chem. Rev. (Washington, D.C.)* **1988**, *88*, 201. Miller, J. S.; Epstein, A. J. *New Aspects of Organic Chemistry*; Yoshida, Z., Shiba, T., Ohsiro, Y., Eds.; VCH Publishers: New York, 1989; p 237. Miller, J. S.; Epstein, A. J. *Angew. Chem., Int. Ed. Engl.* **1994**, *33*, 385; *Angew. Chem.* **1994**, *106*, 399. Miller, J. S.; Epstein, A. J. *Adv. Chem. Ser.* **1995**, *245*, 161.

(4) Manriquez, J. M.; Yee, G. T.; McLean, R. S.; Epstein, A. J.; Miller, J. S. *Science* **1991**, *252*, 1415. Miller, J. S.; Yee, G. T.; Manriquez, J. M.; Epstein, A. J. Conjugated Polymers and Related Materials: The Interconnection of Chemical and Electronic Structure. In *The Proceedings of Nobel Symposium #NS-81*; Oxford University Press: Oxford, 1993; p 461; *Chim. Ind.* **1992**, *74*, 845. Epstein, A. J.; Miller, J. S. Conjugated Polymers and Related Materials: The Interconnection of Chemical and Electronic Structure. In *The Proceedings of Nobel Symposium #NS-81*; Oxford University Press: Oxford, 1992; p 475; *Chim. Ind.* **1993**, *75*, 185. Zhang, J.; Zhou, P.; Brinckerhoff, W. B.; Epstein, A. J.; Vazquez, C.; McLean, R. S.; Miller, J. S., *A.C.S. Sym. Ser.* **1996**, *644*, 311.

S0002-7863(97)03452-5 CCC: $15.00
Published on Web 02/03/1998

Table 1. Summary of the Structural and Magnetic Parameters for the $[TCNE]^{\bullet-}$ Salts of **1**−**5**

porphyrin	Mn−N_{TCNE} distance, Å	Mn−N−C angle, deg	dihedral angle, deg	Mn···Mn distance,[a] Å	effective θ, K	T_{min}, K
MnTPP (**1**)[b]	2.327	146.8	55.1	10.116	61	270
MnTClPP (**2**)	2.267	167.2	86.8	10.189	13	110
MnTOMePP (**3**)	2.289	165.5	78.1	10.256	21	134
MnTFPP (**4**)[b]	2.309	150.3	55.6	10.185	45	240
MnTP′P (**5**)	2.298	128.9	30.4	8.587	90	>300[c]
average	2.298	151.7	61.2	9.866	48	>211

[a] Intrachain. [b] Major orientation. [c] Not plotted.

The high T_c of the $V(TCNE)_x$ magnet demonstrates the great utility of using metal ion/organic radical systems in the design of new ordered molecular materials. The concept of utilizing potentially multidentate organic radicals which may bond directly to open-shell metal centers, however, has been used to a limited extent in the synthesis of new molecule-based magnets.[4,5] Since these types of materials can exhibit strong nearest-neighbor interactions (due to direct metal−radical interactions) as well as high critical temperatures (due to multidimensional interactions), we have sought related TCNE-based materials which may allow correlation of the molecular structure with the strength of magnetic coupling. Correlations between magnetic coupling and molecular structure have been developed for binuclear metal complexes (such as hydroxy-bridged Cu−Cu complexes)[6] and metal−radical complexes in which Gatteschi and co-workers examined the effects of orbital overlap on spin coupling in nonordering, isolated Cu^{II} [7a] and Mn^{II} [7b] nitroxide complexes. In these cases, however, diamagnetic species were substituted in place of the radical to simplify the extended Huckel calculations. However, detailed correlations have not been determined for ordered molecule-based magnetic systems. From these relationships, the important structural features which control T_c could be determined in order to provide guidance for the future design of such materials.

The [MnTPP][TCNE] class of linear chain ferrimagnets[8−11] (Table 1) display strong short-range coupling and weaker 3D long-range order and are particularly amenable to the development of such correlations. This is due in part to the ease with which the porphyrin macrocycle can be modified, thereby inducing changes in the structure and the magnetic order. Additionally, single crystals were obtainable as di-toluene solvates allowing the determination of their molecular structures. Herein, we report a comprehensive examination of the orientation of $[TCNE]^{\bullet-}$ bound to a $[Mn^{III}(por)]^+$ and correlate it with the magnetic data. The observed behavior is examined by considering the orbital overlap between the singly occupied molecular orbitals (SOMO) on $[TCNE]^{\bullet-}$ (π^*) and the four Mn(III)-centered d-orbital SOMOs as determined by semiempirical INDO/SCF calculations. Correlating these changes with the resultant magnetic properties should facilitate the development of new higher T_c molecule-based magnets.

Experimental Section

The SOMOs of both the $[Mn^{III}(por)]^+$ and $[TCNE]^{\bullet-}$ units have been calculated using a restricted open-shell Hartree−Fock (ROHF) version of the INDO method developed by Böhm and Gleiter[12] which employs a single-ζ Slater atomic orbital (AO) basis set for the valence orbitals. Although this approach is not the most sophisticated, it correctly reproduces the trends of the SOMO−SOMO overlaps as a function of the geometric arrangement of the interacting units. Unfortunately, even ab initio versions of the ROHF method do not reproduce the experimental values of the spin density on $[TCNE]^{\bullet-}$ with sufficient numerical accuracy, as the calculated spin densities on the terminal nitrogens are too small.[13] We therefore use the half-electron method[14] for the calculation of the SOMO of $[TCNE]^{\bullet-}$ which is in better agreement with the experimental results than the standard ROHF method in this particular case. The $[Mn^{III}(por)]^+$ and $[TCNE]^{\bullet-}$ geometries were taken from the structural data,[8−11] except that the *meso*-Ph's were replaced by H's to simplify the calculations.

The SOMOs are obtained by separate SCF calculations for each of the $[Mn^{III}(por)]^+$ and $[TCNE]^{\bullet-}$ structural units with the AO's denoted as ϕ_μ^{MnP} and ϕ_ν^{TCNE}, respectively. The SOMOs (Ψ) are given by linear combinations of these AO's:

$$\Psi_i^{MnP} = \sum_\mu \phi_\mu^{MnP} c_{\mu i}^{MnP}$$

$$\Psi^{TCNE} = \sum_\nu \phi_\nu^{TCNE} c_\nu^{TCNE} \qquad (1)$$

The MO coefficients (c) are determined separately for both units. Note that we have one $[TCNE]^{\bullet-}$ SOMO, but four $[Mn^{III}(por)]^+$ SOMOs, thus i in eq 1 ranges from 1 to 4. The overlap of the SOMOs on the two units is of particular importance with respect to the magnetic interactions. The overlap integral, S, between one of the SOMO's on $[Mn^{III}(por)]^+$ and the SOMO of $[TCNE]^{\bullet-}$ is

$$S_i = \langle \Psi_i^{MnP} | \Psi^{TCNE} \rangle = \sum_\mu \sum_\nu c_\nu^{TCNE} c_{\mu i}^{MnP} \langle \phi_\mu^{MnP} | \phi_\nu^{TCNE} \rangle \qquad (2)$$

Our analysis of the SOMO−SOMO overlap includes all Mn 3d AO's, except $d_{x^2-y^2}$, Mn 4s and the N p_z AO's of the porphyrin nitrogens, and the p AO's of the nitrogen closest to Mn for $[TCNE]^{\bullet-}$. (The contributions of the porphyrin C atoms to the $[Mn^{III}(por)]^+$ SOMO are negligible.) These give the dominant contributions to the SOMO−SOMO overlap for all compounds. The coordinate system with its origin in the center of the porphyrin ring has been chosen such that the z axis is perpendicular to the porphyrin plane and that the four pyrrole nitrogens lie on the x and y axes. The p orbitals of the $[TCNE]^{\bullet-}$ N bonded to Mn are denoted as p_x, p_y, and p_z. π overlap occurs between the p_x and d_{xz} as well as the p_y and d_{yz} orbitals, and σ overlap occurs between the p_z and d_{z^2} orbitals. When the dihedral angle, ϕ, between the $[TCNE]^{\bullet-}$ and MnN_4 mean planes is 90° the σ overlap does not contribute to the SOMO−SOMO overlap integrals as the p_z does not have a component to the π^* orbital. When ϕ is less than 90° the p_z

(5) Inoue, K.; Iwamura, H. *Adv. Mater.* **1996**, *8*, 73. Iwamura, H., *Pure Appl. Chem.* **1996**, *68*, 243.
(6) Crawford, V. H.; Richardson, H. W.; Wasson, J. R.; Hodgson, D. J.; Hatfield, W. E. *Inorg. Chem.* **1976**, *15*, 2107.
(7) (a) Caneschi, A.; Gatteschi, D.; Grand, A.; Laugier, J.; Pardi, L.; Rey, P. *Inorg. Chem.* **1988**, *27*, 1031. (b) Caneschi, A.; Gatteschi, D.; Laugier, J.; Pardi, L.; Rey, P.; Zanchini, C. *Inorg. Chem.* **1988**, *27*, 2027.
(8) Miller, J. S.; Calabrese, J. C.; McLean, R. S.; Epstein, A. J. *Adv. Mater.* **1992**, *4*, 498.
(9) Böhm, A.; Vazquez, C.; McLean, R. S.; Calabrese, J. C.; Kalm, S. E.; Manson, J. L.; Epstein, A. J.; Miller, J. S. *Inorg. Chem.* **1996**, *35*, 3083.
(10) Brandon, E. J.; Arif, A. M.; Miller, J. S. Submitted for publication.
(11) Brandon, E. J.; Arif, A. M.; Burkhart, B. M.; Miller, J. S. Submitted for publication.
(12) Böhm, M. C.; Gleiter, R. *Theor. Chim. Acta* **1981**, *59*, 127.
(13) Zheludev, A.; Grand, A.; Ressouche, E.; Schweizer, J.; Morin, B. G.; Epstein, A. J.; Dixon, D. A.; Miller, J. S. *J. Am. Chem. Soc.* **1994**, *116*, 7243.
(14) Dewar, M. J. S.; Hashmall, J. A.; Venier, C. G. *J. Am. Chem. Soc.* **1968**, *90*, 1953.

Table 2. SOMO Overlap Integrals between Mn^{III} d_{yz}-, d_{xz}-, d_{xy}-, and d_{z^2}-like and the $[TCNE]^{\bullet-}$ [a] π^* Orbitals

porphyrin	d_{yz}-like[b] (π)	d_{xz}-like[b] (π)	d_{xy}-like[b] (δ)	d_{z^2}-like[b] (σ)	ΣS^2
TPP (**1**)	0.000 759 97	0.000 240 81	0.000 279 30	0.009 087 8	0.000 083 3
TClPP (**2**)	0.000 207 62	0.000 089 75	0.000 151 47	0.001 303 3	0.000 001 773
TOMePP (**3**)	0.000 007 290	0.000 080 140	0.000 165 97	0.004 020 3	0.000 016 197
TFPP (**4**)	0.000 354 64	0.000 701 66	0.000 409 42	0.009 902 3	0.000 098 84
TP′P (**5**)	0.001 468 8	0.003 908 0	0.000 304 58	0.013 875	0.000 210 04

[a] Determined using the half-electron method. [b] Dominant d orbital coefficients. Symmetry is in parentheses.

Table 3. p_x, p_y, and p_z AO Coefficients (c) of the $[TCNE]^{\bullet-}$ π^* SOMO for the N AO's Bonded to the Mn^{III}

porphyrin	p_x	p_y	p_z
MnTPP (**1**)	0.1573	0.0657	−0.1155
MnTClPP (**2**)	−0.1849	0.1273	−0.0165
MnTOMePP (**3**)	−0.1734	0.1355	0.0473
MnTFPP (**4**)	0.1563	−0.0849	0.1265
MnTP′P (**5**)	0.1010	−0.0955	−0.1766

component to the $[TCNE]^{\bullet-}$ π^* orbital becomes finite (as cos ϕ) and is of correct symmetry to have σ overlap with the d_{z^2} orbital. There is no δ overlap because the $[Mn^{III}(por)]^+$ SOMO with predominant d_{xy} character lacks an AO of appropriate symmetry on the nearest-neighbor nitrogen of $[TCNE]^{\bullet-}$ with which it can overlap. This is confirmed by the numerical values[15] shown in Table 2. Therefore we restrict our considerations to the σ (d_{z^2}/p_z) and π (d_{xz}/p_x, d_{yz}/p_y) overlaps. Hence, the σ and π contributions to the SOMO−SOMO overlap are determined by the p_z, p_x, and p_y AO coefficients of the π^* SOMO of $[TCNE]^{\bullet-}$, respectively, Table 3. The relevance of these overlap integrals for the magnetic intrachain coupling is discussed below.

Results

Structure. The correlations reported here between the orientation of $[TCNE]^{\bullet-}$ bound to a $[Mn^{III}por]^+$ is based upon tetraphenylporphyrin (= por) (H_2TPP, **1**), tetrakis(4-chlorophenyl)porphyrin (H_2TClPP, **2**), tetrakis(4-methoxyphenyl)-porphyrin ($H_2TOMePP$, **3**), tetrakis(2-fluorophenyl)porphyrin (H_2TFPP, **4**), and tetrakis(3,5-di-*tert*-butyl-4-hydroxyphenyl)-porphyrin ($H_2TP'P$, **5**). These five $[Mn^{III}(por)]^+[TCNE]^{\bullet-}$ salts have been characterized as the ditoluene solvates by single-crystal X-ray diffraction,[8−11] and all are structurally related possessing linear chains of $[Mn(por)]^+$ cations bridged by $[TCNE]^{\bullet-}$ in a *trans*-μ-N-σ-fashion, forming coordination polymers with an $\cdots A^+B^-A^+B^-A^+B^-\cdots$ (A = Mn(por); B = TCNE) motif, e.g., Figure 1. (Additionally, all five structures belong to the centrosymmetric $P\bar{1}$ space group with $Z = 1$.) Each structure, however, has $Mn-N_{TCNE}$ distances that range from 2.267 to 2.316 Å, intrachain Mn···Mn separations that range from 8.587 to 10.256 Å, Mn−N−C angles that range from 128.9 to 167.2°, and MnN_4-$[TCNE]^{\bullet-}$ mean-plane dihedral angles, ϕ, ranging from 30.4 to 86.8°, Table 1. This corresponds to variations of 2.6, 16.9, 25.2, and 92.1%, respectively, from the mean values. Hence, substitution of the porphyrin ring with various pendent groups influences the overall solid-state packing.

Magnetic Data. DC SQUID magnetic susceptibility measurements as a function of temperature have been reported for compounds **1**−**5**.[8−11] The data were taken on samples measured directly after filtration from the solution, to avoid aging phenomena and loss of solvent. The moment and χT as a function of temperature all display the same general trend, i.e., a drop in value as the temperature is reduced until a broad minima is reached. The temperature at which these minima (T_{min}) occur indicate the presence of antiferromagnetic coupling,[16] and stronger intrachain coupling is reflected in a larger T_{min}. T_{min} may occur above room temperature as noted for **5**. Hence, T_{min} is correlated with the structure and overlap for **1**−**4** data (vide infra). Below T_{min}, the moment (and χT) rises rapidly with decreasing temperatures and reaches a maximum prior to a rapid reduction in the value of the moment, due to the onset of zero field splitting. When the minimum occurs above 300 K it may be estimated from fitting the data to the Seiden expression for the magnetic behavior of isolated chains of alternating quantum ($S = {}^1/_2$) and classical ($S > {}^1/_2$) spins.[17] However, for **5** $\chi T(T)$ cannot be adequately modeled by the Seiden expression; hence, T_{min}, which exceeds 300 K, cannot be estimated and is not plotted. Due to the broadness of the minima as well as slight variations observed between samples, the accuracy of the positions are estimated at ca. ±20 K. Nonetheless, T_{min} varies from 110 to above 300 K corresponding to a variation of greater than 90% from the mean value, Table 1, and has an inverse linear correlation with the dihedral angle between the MnN_4 $[Mn(por)]^+$ plane and the $[TCNE]^{\bullet-}$ mean plane, Figure 2. On the basis of the linear fit to the data for **1**−**4** and the known dihedral angle for **5**, T_{min} is estimated to be ∼350 K from Figure 2, consistent with the observed data.

In contrast to the temperature dependence of the moment and χT, the temperature dependence of the reciprocal susceptibility, χ^{-1}, for this class of materials, in principle, has two linear regimes which can be fitted to the Curie−Weiss expression, $\chi \propto (T - \theta)^{-1}$ where θ is obtained as the T at which the extrapolated line intercepts the abscissa, and $\theta > 0$ reflects

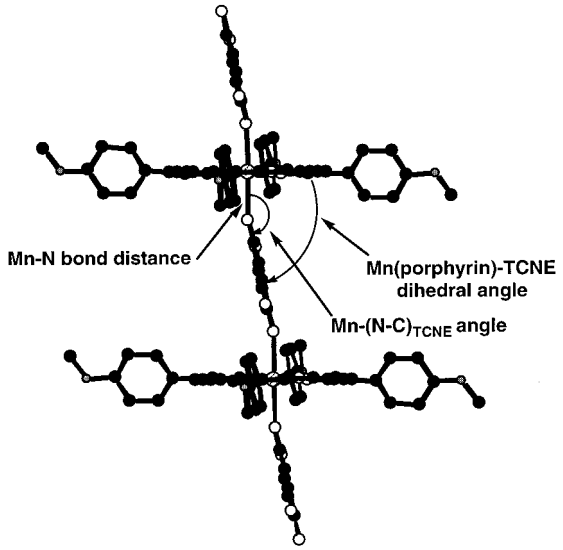

Figure 1. Representative $\cdots A^+B^-A^+B^-A^+B^-\cdots$ chain segment of [Mn(por)][TCNE]·2PhMe, indicating the key bonding parameters. View is taken parallel to both the $[TCNE]^{\bullet-}$ and the porphyrin plane, to emphasize the dihedral angle.

(15) The very small nonzero value of this overlap integral arises from small symmetry deviations and from contributions neglected in our simplified analysis.

(16) For example: Verdaguer, M.; Julve, M.; Michalowicz, A.; Kahn, O. *Inorg. Chem.* **1983**, *22*, 2624. Drillon, M.; Gianduzzo, J. C.; Georges, R. *Phys. Lett. A*, **1983**, *96A*, 413. Kahn, O. *Struct. Bonding* **1987**, *68*, 89.

(17) Seiden, J. *J. Phys. Lett.* **1983**, *44*, L947.

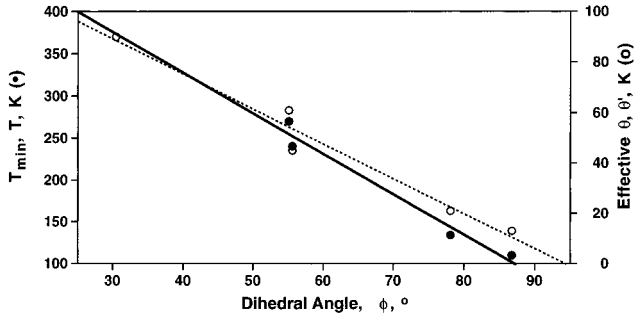

Figure 2. Correlation of the dihedral angle, ϕ, between the MnN_4 and [TCNE]$^{\bullet-}$ mean planes with the temperature that χT has a minimum, T_{min}, and the effective θ value, θ'.

ferromagnetic coupling and $\theta < 0$ reflects antiferromagnetic coupling. Due to the intrachain antiferromagnetically coupling the higher temperature linear region has $\theta < 0$, while the lower temperature linear region has $\theta > 0$. The lower temperature, θ, is termed an effective Curie−Weiss constant or effective θ, θ'. θ' for **1**−**5** varies from 13 to 90 K corresponding to a variation of greater than 150% from the mean value, Table 1, and has an inverse linear correlation with the dihedral angle between the MnN_4 [Mn(por)]$^+$ plane and the [TCNE]$^{\bullet-}$ mean plane, Figure 2.

Discussion

With the premise that the orbital overlap between the Mn^{III} SOMO's and the [TCNE]$^{\bullet-}$ SOMO are important for the intrachain magnetic coupling constant, *J*, calculations of these overlaps as a function of the structurally observed orientations[8−11] between [TCNE]$^{\bullet-}$ bound to [Mn(por)]$^+$ for **1**−**5** were undertaken. The overlap integral is related to the *J* as $J = 2K + 4\beta S$ where *K* is the exchange integral, β is the resonance or bond integral, and *S* is the overlap integral. Since these SOMO's are nonorthogonal, the antiferromagnetic contribution ($4\beta S$) to *J* is assumed to be dominant and theferromagnetic contribution (*K*) is ignored. By using the Wolfsberg−Helmholz approximation ($\beta \sim S$),[18] S^2 is proportional to *J*. Since all minima of the moments occur above 110 K, the much weaker interchain couplings are only important below 40 K and are ignored.

The electronic structure for idealized d^4 [Mn^{III}(por)]$^+$ is d_{xy}^1 (b_1) < d_{xz},^{1} d_{yz}^1 (e) < $d_{z^2}^1$ (a_1) < $d_{x^2-y^2}^0$ (b_1).[19] Due to the [TCNE]$^{\bullet-}$ bonding to Mn^{III}, the symmetry is lowered and the d_{xz}^1 and d_{yz}^1 orbitals are no longer degenerate. Since the dihedral angles, ϕ, between the mean [Mn(por)]$^+$ and the [TCNE]$^{\bullet-}$ planes are intermediate between 0 and 90°, the π* [TCNE]$^{\bullet-}$ SOMO may overlap with the [Mn(por)]$^+$ SOMO's of σ (d_{z^2}) and π (d_{xz}, d_{yz}) symmetry. Since the δ overlap can be neglected (vide supra), there are three interactions between the Mn^{III} and [TCNE]$^{\bullet-}$ which may lead to coupling of the unpaired spins (π-d_{xz}/p_x, π-d_{yz}/p_y, and σ-d_{z^2}/p_z) It should be noted that the p_π AO of the terminal nitrogen of [TCNE]$^{\bullet-}$ bonded to Mn(III) is neither a pure σ nor a pure π orbital with respect to the bond Mn−N, Table 3.

Hence, to estimate *J* the overlap integral (*S*) between each of the four porphyrin SOMOs (*A*) (which are mainly d in character) and the [TCNE]$^{\bullet-}$ π* SOMO (*B*) is calculated. The antiferromagnetic part of the magnetic coupling between two units *A* and *B* with several SOMO's on each of them is

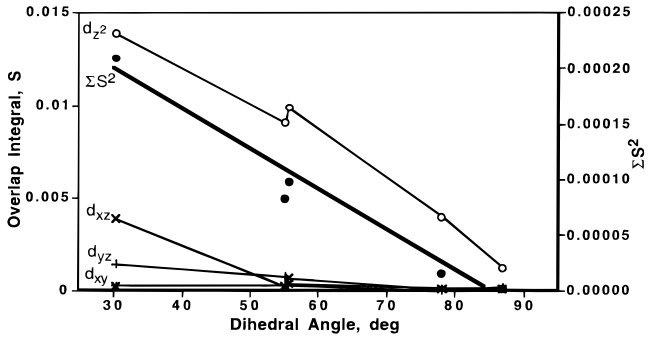

Figure 3. Correlation of the dihedral angle between the MnN_4 and [TCNE]$^{\bullet-}$ mean planes with the calculated d_{yz}-, d_{xz}-, d_{xy}-, d_{z^2}-like overlap integrals, *S*, with the [TCNE]$^{\bullet-}$ π* SOMO, and the sum of the squares of these overlap integrals, $\sum S^2$.

proportional to $\sum_{i\in A}\sum_{j\in B}\beta_{ij}S_{ij}$.[20] Again using the Wolfsberg−Helmholz approximation ($\beta_{ij} \sim S_{ij}$), the relevant quantity for the antiferromagnetic coupling is the sum of the squared overlap integrals $\sum_{i\in A}\sum_{j\in B}S_{ij}^2$, Table 2.

Comparison of the calculated S's (Table 2) and geometric parameters for **1**−**5**, Table 1, reveals that the σ contribution arising from the d_{z^2}/p_z overlap increases with decreasing dihedral angle (ϕ) between the porphyrin and the [TCNE]$^{\bullet-}$ mean planes, Table 2, Figure 3. From the coefficients given in Table 3 one would expect the π contribution to dominate the SOMO−SOMO overlap for $\phi \sim 90°$, i.e., [MnTOMePP]$^+$ and [MnTClPP]$^+$ salts as ϕ approaches 90°. This, however, is not the case as can be seen from Table 2 and Figure 3. Contrary to expectation, the π overlap even decreases with increasing dihedral angle. Obviously, this model is oversimplified and a more detailed analysis of the [Mn^{III}(por)]$^+$ SOMOs is necessary.

The σ SOMO has a d_{z^2} contribution of ~83%, whereas the π SOMO's have d_{xz} and d_{yz} contributions of somewhat less than 70% each. The remaining 30% is, of course, located on the porphyrin ligand, primarily on two of the four nitrogens (~10% each). Thus, the π SOMO's have an antibonding admixture of N p_z orbitals, i.e., **6**.

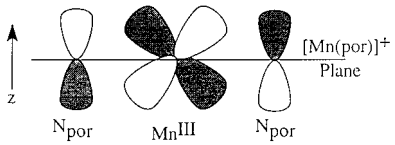

Hence, the p_x and p_y AO's on the terminal nitrogen of [TCNE]$^{\bullet-}$ do not only overlap with, respectively, d_{xz} and d_{yz}, but also with the symmetry-adapted linear combination of the N p_z AO's, **6**. Although these N AO's have considerably smaller coefficients than d_{xz} or d_{yz} in the corresponding SOMO's and these nitrogens are further apart from the [TCNE]$^{\bullet-}$ nitrogen than Mn, their overlap with the p_x or p_y orbitals of the [TCNE]$^{\bullet-}$'s N bound to Mn cannot be neglected because the N p_zAO's are much more diffuse than the metal 3d AO's. This overlap is not only of opposite sign (cf. **6**), but has also almost the same absolute value as the d_{xz}/p_x or d_{yz}/p_y overlaps. Thus, the two opposite effects approximately cancel each other.

For [MnTClPP][TCNE] the π overlap is expected to be most important due to $\phi \sim 90°$. The contribution of the d_{yz}/p_y overlap in eq 2 to the total SOMO−SOMO overlap integral is calculated to be −0.002 68 whereas the contribution of the overlap between the N(porphyrin) p_z AO's and p_y is calculated to be +0.002 99.

(18) Wolfsberg, M.; Helmholz, L. *J. Chem. Phys.* **1952**, *20*, 837.
(19) Dugad, L. B.; Behere, D. V.; Marathe, V. R.; Mitra, S. *Chem. Phys. Lett.* **1984**, *104*, 353.
(20) Girerd, J. J.; Charlot, M. F.; Kahn, O. *Mol. Phys.* **1977**, *34*, 1063. Kollmar, C.; Kahn, O. *J. Chem. Phys.* **1993**, *98*, 453.

The difference between the absolute values of these two values is an order of magnitude smaller than the values themselves and is comparable to overlap effects neglected in our simplified picture. This is also true for **1** and **3**−**5**. Hence, we can even neglect the π overlap for compounds with $\phi \sim 90°$ and consider primarily the σ overlap between d_{z^2} and the p_z component of the π^* SOMO.

In contrast to the π overlap, the σ overlap shows the expected behavior as a function of ϕ. From the data in of Tables 2 and 3, a correlation between the σ SOMO−SOMO overlap integral and the σ component of the π^* SOMO of $[TCNE]^{\bullet-}$ exists. However, in addition to the d_{z^2}/p_z contributing to the SOMO−SOMO overlap, the $4s/p_z$ overlap must be considered as the $3d_{z^2}$ slightly hybridizes with the 4s orbital which contributes to the SOMO by ∼1%. However, since this corresponds to the square of the AO coefficient, the AO coefficient of $3d_{z^2}$ is ∼10 times larger than that of 4s in the SOMO with predominant $3d_{z^2}$ character. As the 4s AO is much more diffuse than $3d_{z^2}$ it gives a nonnegligible (∼30%) contribution to the SOMO−SOMO overlap.

Several correlations between the overlap integrals, *S*, given in Table 2, and geometry data have been identified. (1) $\sum S^2$ increases with decreasing dihedral angle, ϕ,[21] with more acute angles nearly 1 order of magnitude larger than for the higher angle derivatives; and (2) only the overlap integral between $[TCNE]^{\bullet-}$ and a $[Mn(por)]^+$ SOMO predominantly of d_{z^2} character significantly contributes to this sum and also increases with decreasing dihedral angle, ϕ.[21]

This is rationalized by orbital overlap considerations. When ϕ approaches 90°, the $[TCNE]^{\bullet-}$ π^* SOMO becomes orthogonal to the d_{z^2} orbital. As ϕ is decreased, however, overlap can occur between these orbitals, making the $4\beta S$ term more significant and leading to stronger antiferromagnetic coupling. This phenomenon would shift the minima in the moment (and χT) to greater temperature as observed.

(21) A similar correlation is noted for the Mn−N−C angle.

Conclusion

An inverse linear correlation between the crystallographically determined dihedral angle, ϕ, between the MnN_4 and $[TCNE]^{\bullet-}$ mean planes and magnetically determined θ' and T_{min} has been identified. T_{min} is an experimentally determined approximation of J_{intra} and increases over 200 K while θ' increases over 73 K while the angle decreases over 56° for the five ferrimagnets studied. MO calculations also reveal a correlation between ϕ and the SOMO−SOMO overlap and thus the magnetic intrachain coupling as reflected by θ' and T_{min}. Since we restricted ourselves to the dominant antiferromagnetic part of the coupling, a more comprehensive treatment should also include the ferromagnetic exchange integral *K* which was not considered here. These calculations do not provide quantitative values for the coupling constant J_{intra}, but they provide a qualitative trend of the coupling. The key overlap is the $\sigma-d_{z^2}-\pi^*$ overlap between Mn^{III} and the $[TCNE]^{\bullet-}$ not the $d_\pi-\pi^*$ overlap. Thus, they can provide valuable hints to synthetic chemists interested in the tuning of the magnetic intrachain interactions. For example, pressure should force these systems to have reduced ϕ's enhancing the intrachain coupling which can lead to higher T_c's.[22]

Acknowledgment. We gratefully acknowledge stimulating discussions with Professor J. Simons as well as Professor A. J. Epstein, Dr. C. M. Wynn, and Mr. M. Girtu (The Ohio State University) and the support from the National Science Foundation (Grant No. CHE9320478).

JA973452T

(22) Wynn, C. M. Gîrtu, M.; Brinckerhoff, W. B.; Sugiura, K.-I.; Miller, J. S.; Epstein, A. J. *Chem. Mater.* **1997**, *9*, 2156.